Journal of Applied Mechanics and Technical Physics, Vol. 38, No. 2, 1997

CELL MODEL FOR TWO-PHASE MEDIA

P. K. Volkov

UDC 532.529.6

The cell model is attractive because its provides a uniquely simple description for an extremely complicated problem of motion of a liquid mixture with particles or gas bubbles. The main assumption that does not provoke objections when identical particles or bubbles of the same volume are arranged regularly, for example, as uniform identical layers, is that the entire volume can be represented as an aggregate of individual small volumes, i.e., cells containing one particle or bubble [1]. In this case, the determination of motion of a two-phase medium reduces to the solution of ordinary (one-phase) hydrodynamic equations in a region of given form (with a free surface for the bubble). The problem of the interaction of individual particles with each other and with the liquid, which is the main problem in deriving equations of motion of a two-phase medium. becomes the problem of formulating boundary conditions at the outer boundary of the cell which should take into account the presence of surrounding particles (bubbles). The latter is much simpler for justification and realization. The solution of the problem gives a complete description of the internal dynamics of a uniform two-phase medium: floating rate of particles (bubbles) and liquid-velocity distribution over the cell, and, hence, in the mixture as a whole. This information is sufficient to solve problems of practical importance. such as the propagation of heat or admixture in a two-phase medium and the search for the optimal size and optimal density of particles (bubbles) and in the mixture that intensify diffusion processes over the entire volume. The edge effects of the surfaces bounding the mixture are not considered in this paper.

1. Formulation of the Problem. A proper choice of the cell geometry governs the accuracy of modeling the dynamics of a two-phase medium. It follows from the physical notion of the cell that small deviations from the selected cell shape should not change significantly the hydrodynamic characteristics of a bubble or a particle. This is the main premise in selecting the shape of the outer boundary of the cell. For simplicity, we study a two-phase medium with a layered arrangement of bubbles of the same volume.

Let us consider two cases: (a) the bubble layers are located at a distance of $2l$ and the bubbles (points in Fig. 1a) in a layer are uniformly located at the vertices of an equilateral triangle so that each bubble is surrounded by six bubbles; as a cell one can use a right prism of height $2l$ with a regular hexagon in the base and a bubble inside with the center at the middle of the axis passing through the centers of the bases; (b) bubble layers are located at a distance l and bubbles make a checkered packing in space (Fig. 1b) in which each bubble is surrounded by six other bubbles in two levels below and above its center; as a cell one can use a polyhedron of 14 faces with regular hexagons.

Cases (a) and (b) characterize the greatest and least density in the packing, respectively, since the displacement of the liquid which results in floating occurs in case (a) through the smallest cross section between neighboring bubbles.

Let us formulate physical conditions on the cell boundary that would take into account the presence of surrounding bubbles. On the upper and bottom bases, the characteristics should be equal (periodicity conditions), and on the lateral surface, displacement and friction are absent.

The above cell shapes are approximate. The use of these shapes for the calculation of specific problems leads to the necessity of solving complete three-dimensional free-boundary problem for Navier–Stokes equations. At present, this is not a trivial problem, although there are various calculation techniques for these equations. The three-dimensionality in this case is due to the shape of the outer boundary of the

Institute of Thermal Physics, Siberian Division, Russian Academy of Sciences, Novosibirsk 630090.
Translated from Prikladnaya Mekhanika i Tekhnicheskaya Fizika, Vol. 38, No. 2, pp. 115–124, March–April, 1997. Original article submitted August 14, 1995; revision submitted October 2, 1995.

0021-8944/97/3802-0271 $18.00

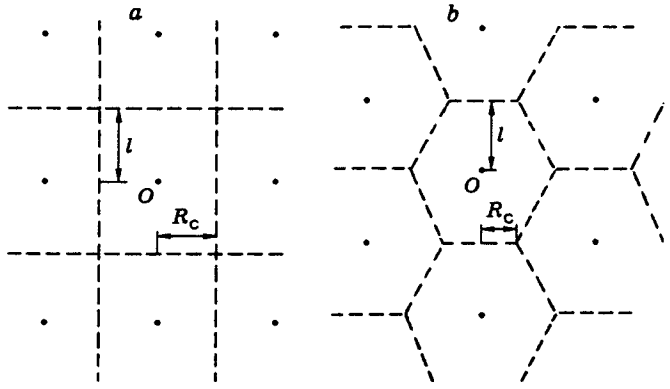

Fig. 1

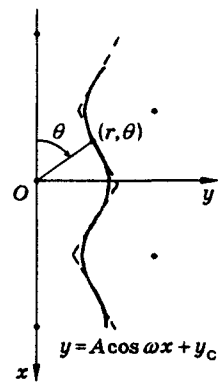

Fig. 2

cell, and it follows from the physical notion of the cell that the cell is a rather stable formation. Therefore, the known procedure of carrying the boundary conditions from the outer boundary of the cell to the given surface is justified. As such surfaces, we shall use surfaces of rotation. This makes it possible to go over from the three-dimensional to the two-dimensional problem, and this is stipulated by the symmetry of bubble arrangement in the layer.

In the mathematical description, it is more convenient to use the coordinate system related to a bubble. In this case, bubbles (and cells) are at rest, and the liquid flows between them. We introduce a spherical coordinate system (r, θ) with the origin at the center of inertia of the bubble. The Navier–Stokes equations describing the motion of a viscous incompressible liquid are written in terms of the stream function ψ and the vortex ω as [2]

$$D^2\psi = -2r\sin\theta\omega; \tag{1.1}$$

$$D^2\omega = \frac{1}{\nu r^2\sin\theta}\left[\psi_\theta\omega_r - \psi_r\omega_\theta - \frac{\omega}{r}\psi_\theta + \omega\operatorname{cotan}\theta\psi_r\right] - \frac{2}{r}\omega_r + \frac{\omega}{r^2\sin^2\theta} - \frac{2\operatorname{cotan}\theta}{r^2}\omega_\theta, \tag{1.2}$$

where

$$D^2 \equiv \frac{\partial^2}{\partial r^2} + \frac{\sin\theta}{r^2}\frac{\partial}{\partial\theta}\left(\frac{1}{\sin\theta}\frac{\partial}{\partial\theta}\right)$$

is the Stokes operator, the subscripts θ and r denote the partial derivatives of the corresponding functions with respect to these variables, and ν is the kinematic-viscosity coefficient.

The following kinematic and dynamic conditions should be satisfied at the free boundary of the bubble Γ $(F(r,\theta) = r - R(\theta) = 0,\ \theta \in [0,\pi])$

$$\mathbf{v}\cdot\nabla F = 0; \tag{1.3}$$

$$\boldsymbol{\tau}\cdot\mathbf{T}\cdot\mathbf{n} = 0; \tag{1.4}$$

$$\mathbf{n}\cdot\mathbf{T}\cdot\mathbf{n} = \sigma K - p_\Gamma. \tag{1.5}$$

Here

$$\mathbf{n} = -\frac{1}{\sqrt{1+(R'/R)^2}}\{1, -R'/R\}, \qquad \boldsymbol{\tau} = -\frac{1}{\sqrt{1+(R'/R)^2}}\{R'/R, 1\}$$

are unit vectors of the normal and tangent to Γ;

$$v_r = \frac{1}{r^2\sin\theta}\frac{\partial\psi}{\partial\theta}, \qquad v_\theta = \frac{-1}{r\sin\theta}\frac{\partial\psi}{\partial r}$$

are the components of the velocity vector $\mathbf{v}$, p_Γ is the gas pressure in the bubble ($p_\Gamma \equiv$ const), $\mathbf{T}$ is the stress tensor, K is the curvature of Γ, and σ is the surface-tension coefficient.

From condition (1.4) we have

$$\frac{1}{2}\left(1-\left(\frac{R'}{R}\right)^2\right)\left(\frac{1}{r}\frac{\partial v_r}{\partial\theta}+\frac{\partial v_\theta}{\partial r}-\frac{v_\theta}{r}\right)+\frac{R'}{R}\left(\frac{\partial v_r}{\partial r}-\frac{v_r}{r}-\frac{1}{r}\frac{\partial v_\theta}{\partial\theta}\right)=0.$$

Taking into account the definition of the vortex

$$\omega=-\frac{1}{2r}\left(\frac{\partial v_r}{\partial\theta}-v_\theta-r\frac{\partial v_\theta}{\partial r}\right)$$

and kinematic condition (1.3), we obtain

$$\omega-\frac{v_\theta(1+2(R'/R)^2-R''/R)}{1+(R'/R)^2}=0. \tag{1.6}$$

Upon similar calculations, we obtain

$$\mathbf{n}\cdot\mathbf{T}\cdot\mathbf{n}=-p+2\rho\nu\left(\frac{\partial v_r}{\partial r}-\frac{R'}{R}\frac{\partial v_\theta}{\partial r}+\frac{R'}{R}\omega\right).$$

Substituting v_r and v_θ, from (1.3)–(1.6) we finally find

$$\psi(R(\theta),\theta)=0; \tag{1.7}$$

$$\omega+\frac{\psi_r}{R^2\sin\theta}\,\frac{1+2(R'/R)^2-R''/R}{1+(R'/R)^2}=0; \tag{1.8}$$

$$-q+\rho gR\cos\theta+2\rho\nu\left[\frac{\psi_{\theta r}-\psi_\theta/R+R'\psi_{rr}}{R^2\sin\theta}+\frac{R'}{R}\omega\right]=p_\infty-p_\Gamma+\sigma K, \tag{1.9}$$

where

$$K=\frac{R^2+2R'^2-RR''}{(R^2+R'^2)^{3/2}}+\frac{|R'\cos\theta-R\sin\theta|}{R\sin\theta(R^2+R'^2)^{1/2}};$$

the primed function $R(\theta)$ denotes differentiation with respect to θ, q is the generalized pressure: $q=p+\rho gR\cos\theta-p_\infty$, p is the pressure, p_∞ is the pressure on the outer cell boundary at the bubble level, g is the acceleration of gravity, and ρ is the density of the liquid.

As in [3], one can show that the periodicity conditions in terms of the stream function ψ and the vortex ω, which reflect the coincidence of the velocity-function values and derivatives over the normal to the boundaries Γ_1 and Γ_2, are of the form (Γ_1 and Γ_2 are the cell bases, and x is the floating direction)

$$\psi\big|_{\Gamma_1}=\psi\big|_{\Gamma_2},\quad \partial\psi/\partial x\big|_{\Gamma_1}=\partial\psi/\partial x\big|_{\Gamma_2},\quad \omega\big|_{\Gamma_1}=\omega\big|_{\Gamma_2},\quad \partial\omega/\partial x\big|_{\Gamma_1}=\partial\omega/\partial x\big|_{\Gamma_2}. \tag{1.10}$$

The nonpenetration condition on the lateral surface of the cell gives $\psi=0$ in the coordinate system of the immovable liquid, since there is no overall discharge of liquid through the section without bubble. In the coordinate system related to the bubble, the flow field is superimposed by the translation with a velocity $-U$, which in the spherical coordinates $(r,\ \theta)$ is described by the function

$$\psi=-Ur^2\sin^2\theta/2. \tag{1.11}$$

Since the conditions on the cell boundary are identical to those on the free boundary, the expressions for the vortex ω can be taken from (1.8), where $R(\theta)$ is a function of the lateral surface.

On the symmetry axis $\theta=0,\ \pi$ we have

$$\psi=\omega=0. \tag{1.12}$$

The algorithm of solution of the boundary-value problem (1.1)–(1.12) practically does not differ from that reported in [2]. The method of realizing the periodicity conditions (1.10) is covered in [4]. The solution of the boundary-value problem in a cell of given geometry is discussed in [5].

This paper is devoted to the problem of choosing the shape of the calculation cell and to the analysis of the results obtained for different bubble packings with the same gas content.

2. Choice of the Calculation-Cell Shape. In Fig. 1a, the calculation-cell shape is obvious: this is a cylinder of height $2l$ (R_c is the radius of the cell base). Since the equation of the generatrix of the surface is $r = R_c/\sin\theta$, for the stream function in (1.11) we obtain the constant $\psi = -UR_c^2/2$. Hence, the lateral surface of the calculation cell is the level surface of the stream function. For other cell configurations, the shape of the lateral surface can be selected in various ways.

As the lateral surface of the cell, one can use a part of the sphere of radius $R_{\text{sphere}} = \sqrt{R_c^2 + l^2}$ that closes the upper and bottom bases of the cell. This is convenient, because $R_{\text{sphere}} = \text{const}$ and the derivatives of the boundary function entering into the transformed equations of motion are equal to zero.

Taking into account the symmetry and periodicity in the arrangement of bubbles in the packing, as the boundary of the calculation cell, one can choose the surface generated by rotation of the curve (Fig. 2)

$$y = A\cos\omega x + y_c. \tag{2.1}$$

Here $\omega = \pi l$ and $y_c = R_c + A$, where A is the cell parameter.

These three types of cell are used in the calculations below. For comparisons to be correct, the parameters of the cells should be matched. Since the bubble volume remains unchanged in the algorithm of solution [2], as a criterion for the selection of the parameters, we use the equality of the volumes of the calculation cells. As initial, data we use the data of [5] for a cylindrical cell with $l = 3$ and $R_c = 3$. Since the dimensionless bubble radius is 2, the volume gas content is 0.2.

Thus, for a cell with a spherical surface, we obtain $R_{\text{sphere}} \simeq 3.46$ and $R_c = \sqrt{3}$, and for cells of the third type, $R_c = (3 + 2l^2/3 - A^2)^{1/2} - A$.

Remark 1. To perform calculations, one should have a description of the cell boundary by a function of the type of $r = G(\theta)$ and know the first and the second derivatives of $G(\theta)$. For cells of the first two types, the derivatives are written analytically. In the third case, $G(\theta)$ is determined by the bisection method as a root of the following transcendental equation for the variable r with a given θ:

$$r\sin\theta = y_c + A\cos(\omega r\cos\theta). \tag{2.2}$$

The derivatives are found by differentiating (2.2) using the values obtained for r:

$$G'(\theta) = (A\sin(\omega r\cos\theta)\omega r\sin\theta - r\cos\theta)/(A\sin(\omega r\cos\theta)\omega\sin\theta + \sin\theta), \quad \text{etc.}$$

Remark 2. The algorithm of numerical solution of [2] includes a change of variables that transforms the flow region with the unknown boundary (bubble) into a quadrangle whose boundaries are parallel to the coordinate lines. As a consequence, the first- and second-order derivatives of the functions describing the boundaries of the flow region appear in the equations. If these functions are not smooth, as is the case at the angles of the cell shapes considered, the derivatives at the angles undergo a discontinuity, which is extended to the line in the calculation domain. Therefore, one should carry out an additional thorough test of the effect of discontinuities in the coefficients of the equations on the calculation results. It is better to test the angles using the problem of flow around a spherical bubble when there are only derivatives of the outer-boundary function in the transformed equations.

The effect of the angles on the numerical solution can be diminished by using curvilinear meshes [6] instead of the evident transformation of the coordinates. In this case, the equations of motion are written for an arbitrary curvilinear coordinate system, and the coordinate system itself is constructed as a solution of another elliptic problem. By virtue of this fact, the effect of the angles is localized.

The simplest realization of the above approach, which makes it possible to study the effect of discontinuities in the equation coefficients on the solution, involves the method of transfinite interpolation of [7], which was used for free-boundary problems [8] in the ideal-fluid model. If $r = G(\theta)$ is the equation of the outer cell boundary and $r = R(\theta)$ is the bubble equation ($\theta \in [0, \pi]$), then the curvilinear coordinates in the flow region are introduced by the formulas

$$r(\xi,\eta) = (1-\eta)G(\xi) + \eta R_p(\xi), \quad \theta(\xi,\eta) = (1-\eta)\pi\xi + \eta G_p(\xi), \quad (\xi,\eta) \in [0,1],$$

where $r = R_p(\xi)$; $\theta = G_p(\xi)$ is a parametric representation of the function $r = R(\theta)$. When $G_p(\xi) = \pi\xi$, the

TABLE 1

R_σ	Fr	Re	We	J	V_m
0.1	0.14	0.64	0.001	20.4	1.0
0.5	4.05	40	2.08	21.1	1.14
1.0	1.75	72	3.52	23.0	1.56

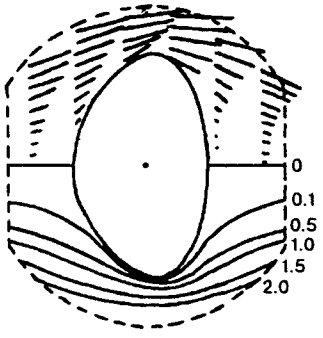

Fig. 3

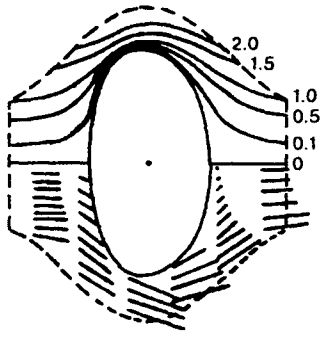

Fig. 4

method of transfinite interpolation is equivalent to the change of variables [2]. The region of reliability of the calculations and the relative degree of the effect of discontinuities of the equation coefficients on the numerical solution are determined by direct comparison of the solutions obtained using these methods.

The use of meshes made it possible to solve problems that could not have been solved previously [5]. Moreover, if the flow region is described by functions with large gradients (the flow region is stretched in one direction), smooth boundaries of the flow region were found to affect strongly the solution.

3. Hydrodynamics of Cells of the Selected Shapes. The mathematical model describing free-boundary viscous flows in a region of specified geometry contains a great number of input constants, which characterize both the physical properties of the medium and the geometry of the flow region. Simulating problems of the stationary rise of bubbles introduces a new constant in the model, namely, the floating rate U, which is not known in advance. The procedures of nondimensionalizing, as a rule, use U as a characteristic velocity. As a result, the equations include a set of dimensionless complexes that are not always independent. Therefore, only upon solving the problem can one determine to which particular medium and bubble size the data obtained correspond. Thus, for the comparison of the results for different cell geometries to be correct, care should be taken to see that the numerical solutions correspond to the same medium and the same linear size of the bubble.

Here, as in [5], $M = \rho^3\nu^4 g/\sigma^3 = \mathrm{We}^3/\mathrm{Fr}\,\mathrm{Re}^4$ is used as a characteristic of the medium and the capillary Laplace constant $\delta_\sigma = (\sigma/\rho g)^{1/2}$ is used as the linear size. Below, the solutions correspond to $M \simeq 2\cdot 10^{-6}$ and the following three values of the length $R_\sigma = a/\delta_\sigma$ [$a = (3V/4\pi)^{1/3}$, where V is the bubble volume]: $R_\sigma = 0.1$, 0.5, and 1.0. The values of the Reynolds number $\mathrm{Re} = U2a/\nu$ and the Weber number $\mathrm{We} = \rho U^2 2a/\sigma$ for which a solution is obtained for the given M (the Froude number $\mathrm{Fr} = U^2/ga$ is the parameter to be determined) are listed below.

Calculations for a Cell with a Spherical Lateral Surface. Table 1 lists data for three radii of a bubble in a cell with the same values of $R_c = \sqrt{3}$ and $R_{\mathrm{sphere}} = 3.46$. Here J is the diffusion of admixture from the bubble [5] and V_m is the maximum velocity of the liquid on the bubble.

The characteristic flow pattern is shown in Fig. 3 ($R_\sigma = 1$, the solid curves are isolines of the stream function, and the dashes represent the liquid-velocity vectors in different sections). For $R_\sigma = 0.1$, the bubble is spherical, and for $R_\sigma = 0.5$, it is somewhat flattened. For $R_\sigma = 0.1$ and 0.5, the values of Fr are much larger than those for a bubble in a single vertical chain with the same distance between the bubble centers, i.e., the

TABLE 2

N	A	R_c	Fr	Re	We	J	V_m	R_σ
			0.04	0.34	0.001	22.7	1.27	0.1
1	1.0	1.43	0.91	18	0.48	24.6	1.53	0.5
			0.69	45	1.4	29.7	2.12	1.0
			0.026	0.28	0.001	21.6	1.12	0.1
2	0.75	2,15	0.89	18	0.44	23.5	1.4	0.5
			0.85	50	1,72	27.4	1.84	1.0
			0.19	0.24	0.001	22.3	1.11	0.1
3	0.5	2.46	0.9	18	0.44	23.5	1.39	0.5
			0.86	50	1.72	26.7	1.87	1.0
			0.44	80	2.0	32.0	2.7	1.6
			0.011	0.18	0.001	23.2	1.25	0.1
			0.84	18	0.44	23.8	1.45	0.5
4	0.25	2.74	0.79	48	1.6	26.3	2.01	1.0
			0.47	70	2.04	31.1	2.6	1.5

presence of surrounding bubbles leads to an increase in the floating rate, which is difficult to interpret from a physical viewpoint. Calculations for other R_c and R_{sphere} (but for the same cell volume) give significant differences in Fr values.

Thus, one can conclude that part of a sphere as the lateral surface of the cell is not a good choice.

Calculations for a Cell with the Lateral Surface Described by (2.1). The results of our calculations for the amplitudes $A = 1$, 0.75, 0.5, and 0.25 with $R_c = 1.43$, 2.15, 2.46, and 2.74, respectively (the same cell volume), are given in Table 2.

Comparison of the Fr, Re, We, J, and V_m values for the same R_σ shows a slight spread of these values for $R_\sigma \geqslant 0.5$. The Fr values are everywhere smaller than those for the case of a single bubble chain with the same l. For bubbles with $R_\sigma \leqslant 1$, flows without separation are still observed, but $R_\sigma = 1$ is likely to be critical: there is a stagnation zone at the trailing part of the bubble (Fig. 4 corresponds to $N = 1$ in Table 2). Whereas for $R_\sigma = 1.1$, there is already a separation which fills the gap between the bubbles near the axis. Figure 5 gives the flow pattern for $N = 3$ and $R_\sigma = 1$ obtained by joining several figures of the same cell along the vertical (the symmetry condition) and from the side (the cosine function is periodic and the superposition is free of clearances). The dashed curves show the cell boundaries.

The flow pattern for Re = 48 and We = 1.6 ($N = 4$ and $R_\sigma = 1$) is close to that presented in Fig. 5. The cell boundary practically repeats the shape of the last isoline of the stream function. This is apparently the most important circumstance that allows one to choose the given cell shape and which is also supported by the velocity distributions on the bubble. Thus, for $N = 1$ and 2 and $R_\sigma \leqslant 0.5$, the profiles are two-humped with a local minimum in the region of the bubble equator. For $N = 3$, the profiles are also two-humped (but with a small amplitude between the local maxima and minima), but only for $R_\sigma = 0.1$. For $N = 4$, the velocity profiles for all R_σ are bell-shaped with a maximum at the equator of the bubble.

Thus, for the given bubble-to-cell volume ratios, the vertical and horizontal distances between the bubbles, and hydrodynamic-parameter values, as a cell for the calculations of the local characteristics of a two-phase medium, one should choose the shape corresponding to $N = 4$ in Table 2.

4. Liquid Dynamics in a Cell of a Two-Phase Medium. The calculations for $N = 4$ (Table 2) for a given R_σ give insight into the motion of the liquid in the cell, and, hence, in a two-phase medium composed of bubbles of the same volume. An increase in R_σ corresponds to liquid mixtures with larger-size bubbles. Since the data are presented for a medium with $M = 2 \cdot 10^{-6}$ and nondimensionalizing was performed over the bubble floating rate U, the ratio of the floating rates of bubbles for the two mixtures denoted by the

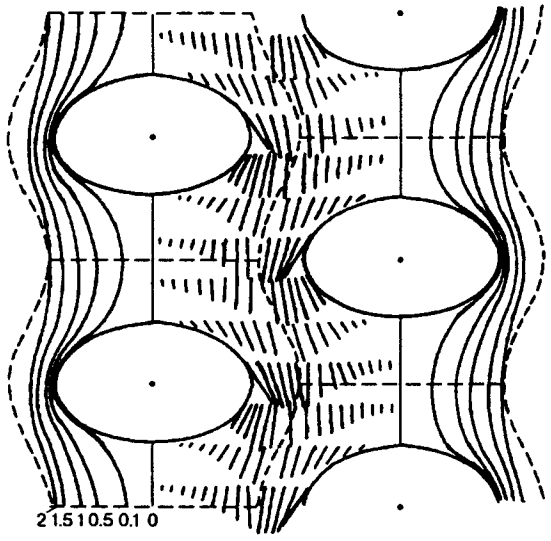

Fig. 5

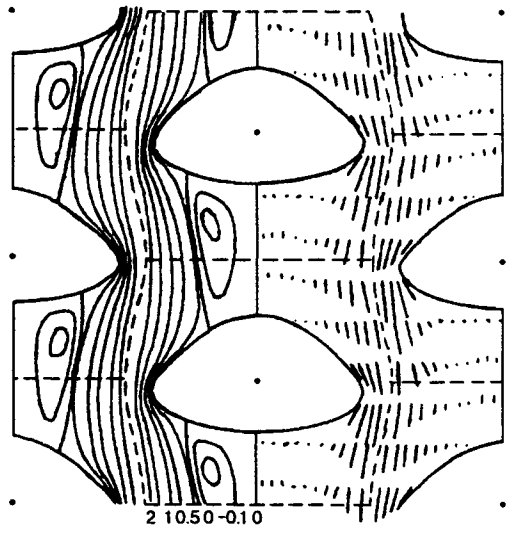

Fig. 6

subscripts 1 and 2 is of the form

$$U_1/U_2 = (\mathrm{Fr}_1 R_{\sigma 1}/\mathrm{Fr}_2 R_{\sigma 2})^{1/2}.$$

For $N = 4$, we obtain

$$U_{0.1}/U_{0.5} \simeq 0.05, \qquad U_{0.5}/U_{1.0} \simeq 0.73, \qquad U_{1.0}/U_{1.5} \simeq 1.06. \tag{4.1}$$

It follows from (4.1) that bubbles whose radius is equal to the capillary constant have the highest floating rate. In this case, we still have flow without separation, as in Fig. 5. There is a separation on bubbles of greater diameter, and a stagnation zone is formed among the bubbles near the axis (Fig. 6). Thus, the bubbles and the part of the liquid between them float. This leads to a decrease in the floating rate. Figure 7 shows graphs of the liquid velocity u on the bubble: curve 1 corresponds to $R_\sigma = 0.1$ (a spherical bubble and Stokes flow), curve 2 corresponds to $R_\sigma = 0.5$ [the bubble is flattened ($\chi \simeq 1.1$) and slight asymmetry appears in the graph], curve 3 corresponds to $R_\sigma = 1.0$ (a stagnation zone exists in the trailing part, but there is no separation yet), and curve 4 corresponds to $R_\sigma = 1.48$ (there are return flows in the region of front points).

Figure 8 shows graphs of $\bar{j}$ (the local diffusion flow of admixture from the bubble surface [5]) that correspond to the above R_σ values. On spherical and slightly deformed bubbles, the maximum is in the region of the leading front point, into which the liquid flows and in which the boundary layer is the thinnest (Stokes flow). As the bubble is deformed, the maximum point is shifted to the equator, where the velocity is maximal. Table 2 presents the overall diffusion J from the bubble. In the presense of separations, the equator region makes the main contribution of 26.86, and the contributions of the leading and trailing parts are 1.35 and 2.91, respectively.

Using the data of Table 2, one can estimate the overall diffusion from systems of bubbles as applied to the problem of bubbling through a liquid layer per unit time. Indeed, the overall diffusion in the volume is proportional to the number of bubbles n. Then, for two systems with different bubbles, the ratio of the overall diffusions $\bar{J}$ is of the form [5]

$$\bar{J}_1/\bar{J}_2 = (a_1 U_1/a_2 U_2)^{1/2}(J_1/J_2)(n_1/n_2)(U_1/U_2). \tag{4.2}$$

The first two cofactors give the ratios of diffusion flows from a single bubble of the systems, the third cofactor gives the ratio of the number of bubbles in the volume considered, and the fourth gives the ratio of the floating rates.

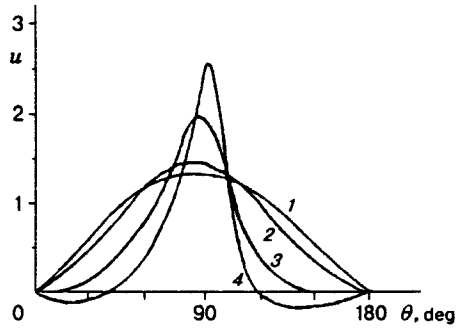

Fig. 7

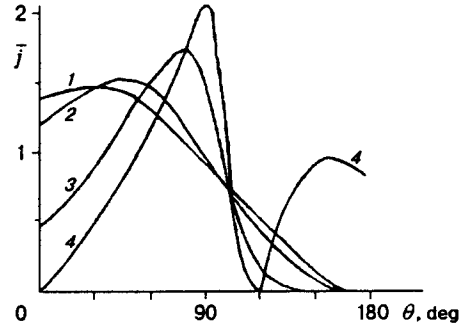

Fig. 8

For the four cases from (4.2), we obtain

$$\bar{J}_{0.1}/\bar{J}_{0.5} \simeq 0.62, \qquad \bar{J}_{0.5}/\bar{J}_{1.0} \simeq 3.2, \qquad \bar{J}_{1.0}/\bar{J}_{1.5} \simeq 2.5. \tag{4.3}$$

It follows from (4.3) that a system with bubbles with a radius of 0.5 of the capillary constant has the largest overall diffusion of the admixture from bubbles to the liquid in the case of bubbling through a liquid unit per unit time.

5. Comparison of Solutions for Two Types of Cell. On the whole, the liquid dynamics in a cylindrical cell (packed as in Fig. 1a) has the same regularities as those described in Sec. 4. Thus, the ratio of floating rates for different R_σ is the same as in (4.1). Flow separation on the bubble occurs even for $R_\sigma = 1$ (but for $R_\sigma = 0.9$ separation does not yet occur). Comparison of the floating rates for different cell types for $R_\sigma = 0.1$, 0.5, 1.0, and 1.5 gives $U_{(b)}/U_{(a)} = 1.2$, 1.2, 1.16, and 1.13, respectively. Thus, the occurrence of a developed vortex wake decreases the difference between the floating rate of bubbles.

Figure 9 shows the flow pattern for $R_\sigma = 1.44$ (Fr = 0.37, Re = 60, We = 1.56, $J = 34$, and $V_m = 3.06$). Figures 6 and 9 correspond to the same medium with a very slight difference in the bubble size. The shape and degree of deformation ($\chi \simeq 1.7$) of the bubbles are practically the same.

For $R_\sigma = 0.5$, the conclusion on the efficiency of a mixture with bubbles for admixture diffusing applied to gas bubbling through the liquid volume remains valid.

Taking into account the aforesaid and the fact that, in going over to the axisymmetric problem, the cell base area is decreased by approximately 10%, and this is the most significant effect on a cylindrical cell (the floating rate decreases), one can speak of practically equal floating rates of bubbles in the mixture. In this case, the requirement of uniform distribution of bubbles in the liquid, which determines the cell geometry and the volume gas content, is of importance.

To determine unambiguously the flow type, floating rate of bubbles, and other integral characteristics. it is insufficient to assign only the average volume gas content ignoring the bubble size.

6. Conclusion. The two cell types considered in the paper transform from one into another upon vertical displacement of one vertical bubble chain relative to six others surrounding the chain. However, with such an arrangement of bubbles, the region is divided into cells that are not almost equivalent. For an adjacent bubble, we obtain the following packing around it: there are three bubbles at the level of the bubble and at the levels that are higher and lower by l. These bubbles are turned through 120°, so that one can see from above a regular hexagon of bubbles. Nevertheless, this can be considered as a cell.

The numerical results suggest that in cells of the same volume and the same height, the integral characteristics of the bubble are the same. A right cylinder can be considered as a cell. If the cell diameter is greater than its height, the effect of the surrounding bubbles in the horizontal layer on the floating rate will be less than that of the bubbles in the vertical chain. For cells whose radius is 4–5 bubble radii, we have an essentially floating chain. For cells whose radius is less than 2 bubble radii, the bubble floating rate depends only slightly on the cell height.

To determine the characteristics of a two-phase medium more exactly, it suffices to clarify the linear dimensions of the cylindrical cell and to perform calculations taking into account the parameter M of the

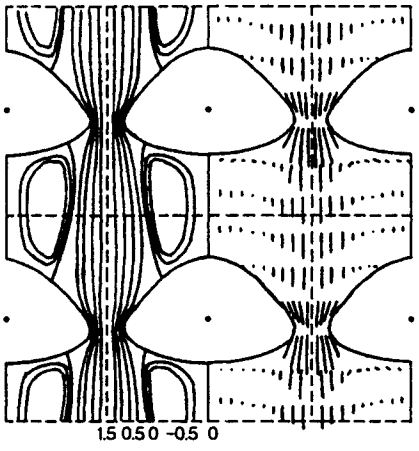

Fig. 9

medium and the bubble volume.

The presence of a maximum in the dependence of the bubble floating rate on its volume is related to flow separation and the appearance of a stagnation zone behind the bubble. The buoyancy force goes to the displacement of part of the liquid together with the bubble.

The extremum properties of the admixture diffusion from the bubble are caused by the disproportional decrease in the floating rate with a decrease in the bubble size as compared with the increase in the number of bubbles with a given volume gas content.

We were unable to obtain stationary solutions for great R_σ. The bubble boundary accomplishes wave-like oscillations, and the iteration process does not converge.

This work was supported by the Russian Foundation for Fundamental Research (Grant No. 95-01-00879a).

REFERENCES

1. R. I. Nigmatulin, *Fundamentals of the Mechanics of Multi-Phase Media* [in Russian], Nauka, Moscow (1978).
2. P. K. Volkov, "The buoyancy of a gas bubble in a tube filled with a viscous liquid," *Prikl. Mekh. Tekh. Fiz.*, No. 6, 98–105 (1989).
3. V. P. Sirochenko, "Numerical solution of one problem of viscous incompressible flow in a double-connected region," in: *Numerical Methods of Continuum Mechanics* [in Russian], Inst. of Theor. and Appl. Mech., Sib. Div., Acad. of Sci. of the USSR, **8**, No. 1, 119–134 (1977).
4. P. K. Volkov, "Motion of a chain of bubbles in a vertical channel with a viscous liquid," *Prikl. Mekh. Tekh. Fiz.*, No. 3, 87–91 (1991).
5. P. K. Volkov and P. I. Geshev, "Hydrodynamics and diffusion of an impurity in a cell of a two-phase medium," *Prikl. Mekh. Tekh. Fiz.*, **36**, No. 6, 68–76 (1995).
6. S. K. Godunov and G. P. Prokopov, "Solution of differential equations using curvilinear difference grids," *Zh. Vychisl. Mat. Mat. Fiz.*, **8**, No. 1, 26–46 (1968).
7. J. F. Thompson, Z. U. A. Warsi, and C. W. Mastin, "Boundary-fitted coordinate systems for numerical solution of partial differential equations (Review)," *J. Comp. Phys.*, **47**, No. 1, 1–108 (1982).
8. P. K. Volkov and Ch. I. Christov, "Numerical simulation of bubble floating in a liquid," *Vychisl. Tekhnol.*, **2**, No. 5, 61–76 (1993).